Control of the bipolarization emission of an Yb:YAG laser by the orientation of the pump polarization

Herman Akagla, Nicolas Chapron, Goulc'hen Loas, Marc Vallet, Marc Brunel

Control of the bipolarization emission of an Yb:YAG laser by the orientation of the pump polarization

HERMAN AKAGLA, NICOLAS CHAPRON, GOULC'HEN LOAS , MARC VALLET, AND MARC BRUNEL

Univ Rennes, CNRS, Institut FOTON–UMR 6082, 35000 Rennes, France

We show that the polarized pumping can be used to control the relative powers of two linear, orthogonally polarized, eigenstates in a Yb:YAG laser. The experimental observations are in full agreement with a two-mode rate-equation model, highlighting the roles of both the gain anisotropy and the cross-saturation parameters, whose values are found to be $\varepsilon = 0.08$ and $\beta = 0.64$, respectively, in a longitudinally pumped contiuous-wave microchip laser. The application to dual-polarization frequency combs is discussed.

Since their first demonstrations more than thirty years ago [1, 2], ytterbium lasers have become ubiquitous in research and technology. Trivalent ytterbium ions in solid-state media provide high quantum efficiency, long fluorescence lifetime, broad absorption and emission ranges. Ytterbium lasers are notably used for ultrashort pulse generation [3], and have recently been shown to provide novel polarization-multiplexed sources for dual-comb spectroscopy [4, 5]. Indeed, when isotropic crystal hosts such as YAG or CaF_2 are used, the generation of two orthogonally polarized eigenstates with different repetition rates is possible. In these examples however, simultaneous oscillation of the two polarizations is obtained at the expense of additional beam displacers in the cavity, in order to avoid cross-saturation effects in the active medium or in the absorber.

While polarization cross-saturation effects have been scarcely studied in ytterbium lasers, it has long been reported in Nd:YAG lasers. In particular the influence of the pump polarization orientation has been experimentally observed [6–8] and theoretically described [9]. Except for the peculiar cases where all anisotropies are rigorously compensated [10], Nd:YAG lasers usually oscillate on two linear orthogonally polarized modes which directions are defined by residual, or voluntarily inserted [11–13], anisotropies. Numerous experiments have shown that the power balance between the two competing polarizations can be controlled by the orientation of the pump polarization, to the advantage of the mode parallel to the pump [6, 7, 9, 14–20]. The cross-saturation parameter plays an important role since the pump-induced gain anisotropy may lead to the complete suppression of one polarization to the benefit of the other. Similar behaviors and analyses emerge in fiber lasers, where the pump orientation also provides an efficient gain anisotropy [21–24].

This raises the question of controlling the dual-polarization oscillation in ytterbium lasers by means of the pump polarization orientation. Indeed, investigating the pump-induced anisotropy and cross-saturation effects could help in designing dual-frequency ytterbium lasers for microwave photonics, or dual-comb sources without beam displacers, for instance. In the lone study reported so far about polarization eigenstates in Yb:YAG lasers, Dong et al. showed experimentally that in an isotropic microchip configuration, the laser polarization also tends to follow the pump [25]. In that study however, simultaneous dual-polarization emission was not clearly evidenced.

In this Letter, we aim to show that the pump polarization provides an efficient gain anisotropy in an Yb:YAG laser, emphasizing the role of the cross-saturation parameter. We wish to compare experimental results obtained with a simple, compact, plano-plano cavity, with a two-mode rate equation model. The model is based on previous literature [22, 26–29], but we aim here to derive pump-dependent stationary solutions with minimal relevant parameters, that are the pump-induced anisotropy parameter and the cross-saturation parameter.

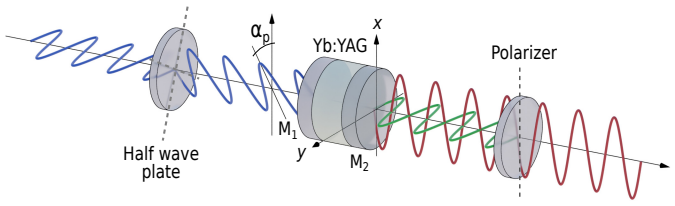

Fig. 1. Illustration of the Yb:YAG laser experimental setup. Laser cavity eigenaxes are labelled x and y. Pump polarization plane is at an angle α_p with respect to x. M_1, M_2: plane cavity mirrors.

The laser used is shown in Fig. 1. The active medium is a 2 mm-thick, <111>-cut, 5% at.-doped, Yb:YAG crystal placed between two plane mirrors M_1 and M_2. The pump mirror M_1 is dichroic (high-reflection at 1030 nm, high-transmission at 940 nm), and output mirror M_2 has a reflectivity of 99% at 1030 nm. The active medium is anti-reflection coated. It is pumped at 940 nm by a continuous-wave Ti:Al_2O_3 laser, which is focused to a spot radius of 17 µm in the active medium. The pump polarization is linear and its orientation is controlled by a half-wave plate. The threshold is reached for a pump power of 80 mW and the laser emits 120 mW at 1030 nm in a TEM_{00} mode for an incident pump power of 1.5 W. A polarizer is inserted before the detection instruments: powermeter, optical spectrum analyser (OSA), Fabry-Perot interferometer (FPI), photodiode. In

order to investigate precisely the polarizations and frequencies of the laser, we analyze the optical spectrum while rotating the polarizer. Although the total spectral envelope contains about a dozen modes evenly-spaced by a free-spectral range of 39 GHz, the polarization-resolved spectra shows two combs of 6 to 8 linear orthogonally-polarized modes (see Fig. 2(a)). These two combs, labelled x and y in the following, overlap partially in the central part of the spectrum. Their spectral separation cannot been seen at this scale with the OSA, but the FPI permits to show that the two combs are actually shifted by about 100 MHz (see $\Delta\nu_{XY}$ in Fig. 2(b)). Note that this small shift reflects the residual birefringence inside the laser, of the order of $\Delta n = 5 \times 10^{-7}$, and we verified that it depends on the pump power - as a result of thermo-optic effects. In addition, we checked that the directions are not affected by the pump polarization. Indeed, by rotating the half-wave plate of the pump, we observe variations in the intensities of the two polarizations, but their directions x and y stay fixed by the residual birefringence of the laser crystal. We will hence consider hereafter that we have two linear "super modes" X and Y oscillating in the laser, each consisting in the superposition of a few longitudinal modes.

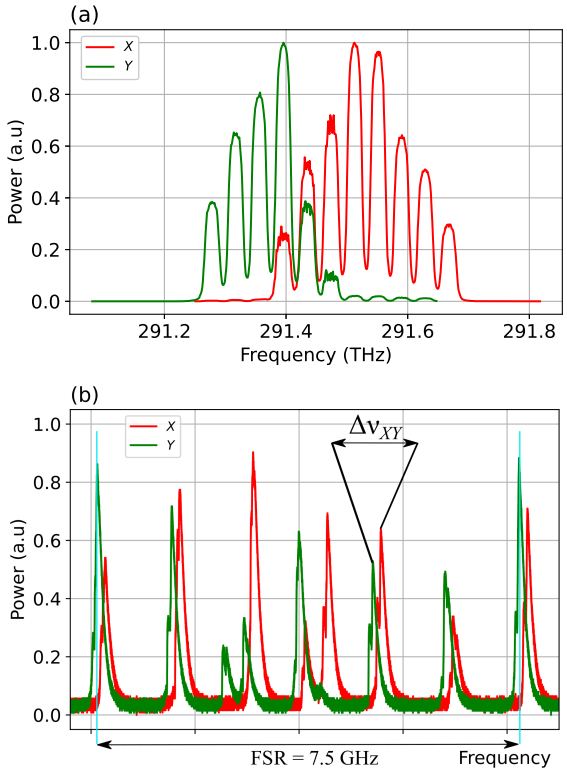

Fig. 2. Polarization-resolved optical spectrum observed with: (a) An optical spectrum analyzer, showing two combs associated with x (red) and y (green) eigenstates; (b) Fabry-Perot scanning interferometer (FPI) revealing the small detuning due to the residual birefringence of the laser. FSR: Free Spectral Range of the FPI.

To model this laser with a minimal number of parameters, let us consider a system of two super-modes characterized by their intensities $I_{x,y}$ interacting with two population inversion reservoirs $n_{x,y}$. Transverse and longitudinal dependencies are neglected (mean-field approximation), as well as phase relationships between modes. It yields four rate-equations [22, 26–29] governing the evolutions of $I_{x,y}$ and $n_{x,y}$:

$$\frac{dI_x}{dt} = \kappa\left(n_x + \beta n_y\right) I_x - \Gamma_x I_x, \tag{1}$$

$$\frac{dI_y}{dt} = \kappa\left(n_y + \beta n_x\right) I_y - \Gamma_y I_y, \tag{2}$$

$$\frac{dn_x}{dt} = \gamma_\parallel P_x - \left[\gamma_\parallel + \zeta\left(I_x + \beta I_y\right)\right] n_x, \tag{3}$$

$$\frac{dn_y}{dt} = \gamma_\parallel P_y - \left[\gamma_\parallel + \zeta\left(I_y + \beta I_x\right)\right] n_y, \tag{4}$$

where Γ_x and Γ_y are the intensity loss coefficients. $\gamma_\parallel$ is the decay rate of the population inversion, κ and ζ are constant atom-field coupling parameters proportional to the emission cross-section, $P_{x,y}$ are the pumping parameters on the x, y polarization states and β is the cross-saturation coefficient coupling the two modes. The gain anisotropy induced by the pumping orientation can take different forms [14, 19, 20, 23, 28]. Following [28], we take

$$P_{x,y} = P\left(1 \pm \varepsilon\cos\left(2\alpha_p\right)\right), \tag{5}$$

where P is half the total population inversion, ε is the pump-induced gain anisotropy parameter, and α_p is the angle of the pump polarization with respect to x. The physical picture can be understood as a preferential pumping of ions located in the crystal sites where dipoles are parallel to the pump; consequently stimulated emission also comes preferentially from those sites. Using the set of eqs. (1) to (4) with Eq. (5), let us now describe the intensities with respect to the pump polarization angle, emphasizing the roles of β and ε. We calculate the stationary solutions of the four coupled equations, making the assumption that the losses on the two polarization states are equal in this microchip configuration, i.e., $\Gamma_x = \Gamma_y = \Gamma$. We introduce normalized expressions for the intensities $\hat{I}_{x,y} = \zeta I_{x,y}/\gamma_\parallel$, and we write the excitation degree $\eta = P/P_{th}$ where the threshold population inversion is $P_{th} = \Gamma/\kappa$. In this study we focus on the solutions where both eigenstates oscillate simultaneously, i.e., modal intensities are non-zero ($\hat{I}_x \neq 0, \hat{I}_y \neq 0$). Stationary solutions are then found to be

$$\hat{I}_{x,y} = \eta\left(1 \pm \varepsilon\frac{1+\beta}{1-\beta}\cos 2\alpha_p\right) - \frac{1}{1+\beta}. \tag{6}$$

It is interesting to note that $\hat{I}_{x,y}(\alpha_p)$ depend on two parameters only: the cross-saturation coefficient β and the pump anisotropy parameter ε, α_p and η being experimental variables. For the sake of analysis, we define as in [20] a contrast parameter which is $r = \hat{I}_y(0)/\hat{I}_x(0)$. In order to see how the relevant parameters of the model affect the intensities of the two modes $\hat{I}_{x,y}$, we calculate Eq. (6) for different values of ε and β and plot the stationary $\hat{I}_{x,y}(\alpha_p)$ as shown in Fig. 3. We observed that the contrast between the two polarization intensities increases when either the pump anisotropy coefficient ε or the cross-saturation parameter β increases. Of course, at low values of η one can find situations where only one mode oscillates, even in our case of equal losses, because of the gain competition described by the β parameter. Besides, it is interesting to note that the parameters β and ε can be determined from experimental measures, as is now detailed.

β can be extracted from the measurement of both the relaxation oscillation frequency (f_R) and the antiphase frequency (f_L) corresponding to the energy exchange between the two polarizations states [22, 26] of the laser. By using an electrical spectrum analyzer, we measure the two frequencies f_L and f_R in the

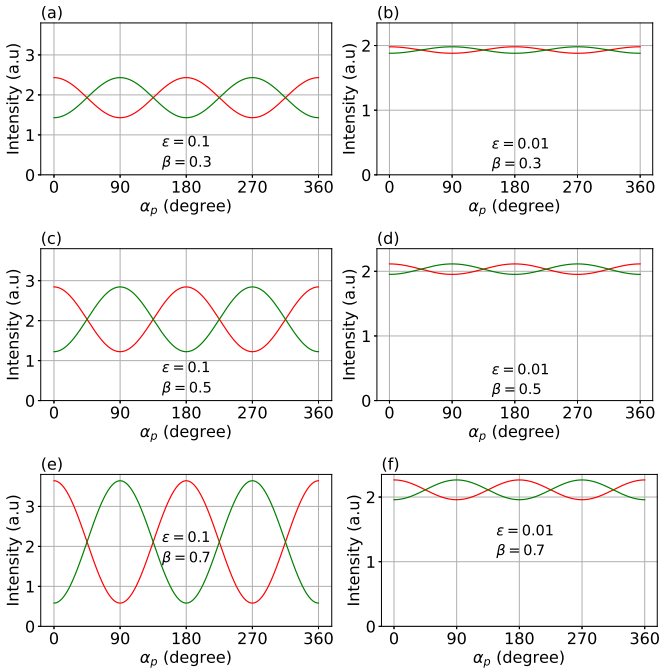

Fig. 3. Theoretical intensities $\hat{I}_x(\alpha_p)$ (in red) and $\hat{I}_y(\alpha_p)$ (in green) at $\eta = 2.7$ for different values of ε and β.

polarization-resolved intensity noise spectrum, as shown in Fig. 4 (both polarizations show the same spectrum). The value of β is then deduced through the equation $\beta = \dfrac{1-h}{1+h}$ where $h = f_L/f_R$. We find $\beta = 0.64 \pm 0.02$. Note that the ratio h can also be related

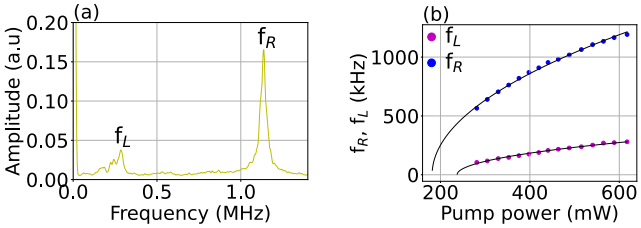

Fig. 4. Antiphase and relaxation frequencies with respect to the input pump power. Points: experimental measurements of f_L and f_R. Solid lines: fits using standard formulas [22].

to a Lamb-type coupling constant $C = \left(\dfrac{1-h^2}{1+h^2}\right)^2$ [30] governing the simultaneity/bistability regimes. Here $C = 0.87 \pm 0.02$. This value of C is quite close to 1, close to bistability conditions, meaning that losses must be well balanced inside such a laser in order to keep the simultaneity regime.

Now, to find out the value of ε, we manipulate Eq. (6) to find

$$\varepsilon = h\frac{(1+\beta)\,\eta - 1}{(1+\beta)\,\eta}\left(\frac{r-1}{r+1}\right), \qquad (7)$$

showing that ε can be determined from the ratio of the experimental powers obtained at $\alpha_p = 0$, once η and β are known. Note that at high pumping rate we have simply $\varepsilon = h\dfrac{r-1}{r+1}$. Fig.5 shows the experimental results of the polarization-resolved powers (associated to x and y combs). When rotating the half-wave plate, hence the pump polarization orientation, we find the periodic energy exchange between the two eigenstates. Fig. 5(a) is plotted when $\eta = 2.7$, while Fig. 5(b) is plotted when $\eta = 18$. In both cases we note an important gain dichroism induced by the polarized pump; for example when $\eta = 2.7$ the power ratio is of the order of 10 at $\alpha_p = 0$ or $\alpha_p = 180°$. In our case, in agreement with the fact that our cavity has no loss dichroism, the polarization balance is obtained for $\alpha_p \equiv 45°\ \pmod{90°}$. Moreover, we observe that the power ratio tends towards a constant value when we move away from the threshold ($r = 2.3$ for $\alpha_p = 0$). In all cases, the total power remains almost constant. Using these results, we deduce from Eq. (7) the value of $\varepsilon = 0.08$.

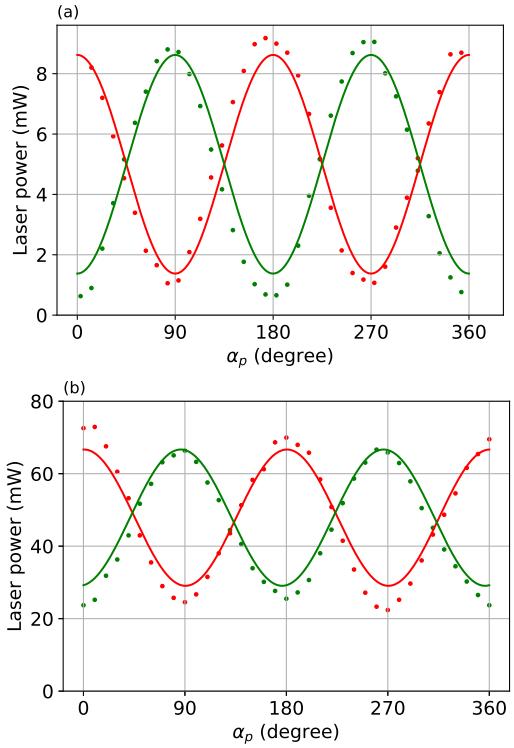

Fig. 5. Powers I_x (in red) and I_y (in green). The points (resp. solid curves) represent the experimental (resp. theoretical) results. (a) $\eta = 2.7$ and (b) $\eta = 18$.

Taking the measured values of our parameters, $\beta = 0.64$ and $\varepsilon = 0.08$, we now compare the model with the experimental results (see the solid lines in Fig. 5). One can notice the very good agreement obtained between the model and the experimental observations for different values of η. The model follows perfectly the evolution of the contrast with respect to the excitation degree.

In order to extend these observations to other laser architecture, we have first pumped the same Yb:YAG microchip laser with a multimode fiber-coupled laser diode. Two lenses are used, one for collimating the fiber output, and another one for focusing inside the active medium. By inserting a polarizer and a half-wave plate between these two lenses, we checked the dependence of x and y intensities versus the pump polarization angle. The results are shown in Fig. 6 for $\eta = 3$, where the simulation curves are obtained with the same parameter values as before, i.e., $\beta = 0.64$ and $\varepsilon = 0.08$. Secondly, we have also studied an extended-cavity architecture, using the same input mirror and active medium, but with a 50 mm radius of

curvature concave mirror placed about 45 mm away from the active medium. In that case again, the eigenstates are linear and orthogonal, and their directions are governed by intracavity anisotropies. All the observations are well-reproduced, showing the ability of the pump polarization to control the power balance between the polarizations in an Yb:YAG laser.

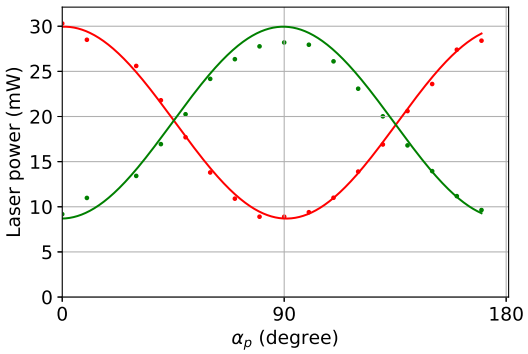

Fig. 6. Powers I_x (in red) and I_y (in green) of the diode-pumped Yb:YAG laser. The points (resp. solid curves) represent the experimental (resp. theoretical) results for $\eta = 3$.

In conclusion, we have shown that the orientation of the pump polarization is an effective tool for controlling the relative powers in bipolarized ytterbium lasers. We have also found values for important parameters that are the cross-saturation and pump anisotropy parameters. Since both parameters are related, at the microscopic level, to the local symmetry of Yb^{3+} ions in the YAG matrix crystal, it would hence be interesting to extend this work to other matrices, such as CaF_2 for instance, or to other crystal orientations in the line of previous work on Nd:YAG lasers [29]. This work can also be extended to dual-polarized short pulse laser architectures [13]. The gain anisotropy induced by the pump orientation could leverage eventual loss anisotropies in more complex cavities used for short pulse generation, in order to optimize the simultaneous oscillation of dual combs in ytterbium lasers.

Funding. This work was partially funded by the CPER SOPHIE-PHOTONIQUE.

Acknowledgments. Technical assistance from Anthony Carré, Ludovic Frein, Steve Bouhier, and Cyril Hamel is gratefully acknowledged.

Disclosures. The authors declare no conflicts of interest.

REFERENCES

1. P. Lacovara, H. Choi, C. Wang, R. Aggarwal, and T. Fan, Opt. Lett. **16**, 1089 (1991).
2. W. F. Krupke, IEEE J. Sel. Top. Quantum Electron. **6**, 1287 (2000).
3. C. Hönninger, G. Zhang, U. Keller, and A. Giesen, Opt. Lett. **20**, 2402 (1995).
4. B. Willenberg, J. Pupeikis, L. M. Krüger, F. Koch, C. R. Phillips, and U. Keller, Opt. Express **28**, 30275 (2020).
5. N. Modsching, J. Drs, P. Brochard, J. Fischer, S. Schilt, V. J. Wittwer, and T. Südmeyer, Opt. Express **29**, 15104 (2021).
6. A. Owyoung and P. Esherick, Opt. Lett. **12**, 999 (1987).
7. J. Lin and M. Yao, Proc. SPIE **1040**, 103 (1989).
8. M. Bergeon, Ph.D. thesis, Université Joseph Fourier – Grenoble 1 (1996).
9. R. Dalgliesh, A. May, and G. Stephan, IEEE J. Quantum Electron. **34**, 1493 (1998).
10. N. V. Kravtsov, E. G. Lariontsev, and N. I. Naumkin, Quantum Electron. **34**, 839 (2004).
11. G. Baxter, J. Dawes, P. Dekker, and D. Knowles, IEEE Photonics Technol. Lett. **8**, 1015 (1996).
12. M. Brunel, F. Bretenaker, and A. Le Floch, Opt. Lett. **22**, 384 (1997).
13. J. Thévenin, M. Vallet, and M. Brunel, Opt. Lett. **37**, 2859 (2012).
14. G. Bouwmans, B. Ségard, and P. Glorieux, Opt. Commun. **196**, 257 (2001).
15. G. Verschaffelt, G. Van der Sande, J. Danckaert, B. Ségard, P. Glorieux, and T. Erneux, Phys. Rev. A **77**, 063801 (2008).
16. K. Otsuka and T. Ohtomo, Laser Phys. Lett. **5**, 659 (2008).
17. K. Otsuka, Opt. Lett. **37**, 4287 (2012).
18. K. Otsuka and S.-C. Chu, Opt. Lett. **38**, 1434 (2013).
19. S. Zhang, Y. Tan, and S. Zhang, J. Opt. **17**, 045703 (2015).
20. H. Chen, S. Zhang, and Y. Tan, Appl. Opt. **55**, 2858 (2016).
21. J. T. Lin and W. A. Gambling, Proc. SPIE **1373**, 42 (1990).
22. S. Bielawski, D. Derozier, and P. Glorieux, Phys. Rev. A **46**, 2811 (1992).
23. R. Leners, P. Françcois, and G. Stephan, Opt. Lett. **19**, 275 (1994).
24. P. A. Khandokhin, Y. I. Khanin, Y. A. Mamaev, N. D. Milovskii, E. Y. Shirokov, S. Bielawski, D. Derozier, and P. Glorieux, Quantum Electron. **28**, 502 (1998).
25. J. Ma and J. Dong, in *Advances in Optical Materials,* (Optica Publishing Group, 2011), p. ATuB27.
26. E. Lacot, F. Stoeckel, and M. Chenevier, Phys. Rev. A **49**, 3997 (1994).
27. M. Brunel, O. Emile, M. Alouini, A. Le Floch, and F. Bretenaker, Phys. Rev. A **59**, 831 (1999).
28. T. Chartier, F. Sanchez, and G. Stéphan, Appl. Phys. B **70**, 23 (2000).
29. S. De, A. El Amili, M. Alouini, and F. Bretenaker, J. Opt. Soc. Am. B **30**, 2830 (2013).
30. M. Brunel, A. Amon, and M. Vallet, Opt. Lett. **30**, 2418 (2005).

FULL REFERENCES

1. P. Lacovara, H. Choi, C. Wang, R. Aggarwal, and T. Fan, "Room-temperature diode-pumped Yb:YAG laser," Opt. Lett. **16**, 1089–1091 (1991).
2. W. F. Krupke, "Ytterbium solid-state lasers. The first decade," IEEE J. Sel. Top. Quantum Electron. **6**, 1287–1296 (2000).
3. C. Hönninger, G. Zhang, U. Keller, and A. Giesen, "Femtosecond Yb:YAG laser using semiconductor saturable absorbers," Opt. Lett. **20**, 2402–2404 (1995).
4. B. Willenberg, J. Pupeikis, L. M. Krüger, F. Koch, C. R. Phillips, and U. Keller, "Femtosecond dual-comb Yb:CaF_2 laser from a single free-running polarization-multiplexed cavity for optical sampling applications," Opt. Express **28**, 30275–30288 (2020).
5. N. Modsching, J. Drs, P. Brochard, J. Fischer, S. Schilt, V. J. Wittwer, and T. Südmeyer, "High-power dual-comb thin-disk laser oscillator for fast high-resolution spectroscopy," Opt. Express **29**, 15104–15113 (2021).
6. A. Owyoung and P. Esherick, "Stress-induced tuning of a diode-laser-excited monolithic Nd:YAG laser," Opt. Lett. **12**, 999–1001 (1987).
7. J. Lin and M. Yao, "Polarization control of diode-pumped Nd:YAG by external fields at various pumping wavelengths," Proc. SPIE **1040**, 103–108 (1989).
8. M. Bergeon, Ph.D. thesis, Université Joseph Fourier – Grenoble 1 (1996).
9. R. Dalgliesh, A. May, and G. Stephan, "Polarization states of a single-mode (microchip) Nd^{3+}:YAG laser. Part II: comparison of theory and experiment," IEEE J. Quantum Electron. **34**, 1493–1502 (1998).
10. N. V. Kravtsov, E. G. Lariontsev, and N. I. Naumkin, "Dependence of polarisation of radiation of a linear Nd: YAG laser on the pump radiation polarisation," Quantum Electron. **34**, 839 (2004).
11. G. Baxter, J. Dawes, P. Dekker, and D. Knowles, "Dual-polarization frequency-modulated laser source," IEEE Photonics Technol. Lett. **8**, 1015–1017 (1996).
12. M. Brunel, F. Bretenaker, and A. Le Floch, "Tunable optical microwave source using spatially resolved laser eigenstates," Opt. Lett. **22**, 384–386 (1997).
13. J. Thévenin, M. Vallet, and M. Brunel, "Dual-polarization mode-locked Nd:YAG laser," Opt. Lett. **37**, 2859–2861 (2012).
14. G. Bouwmans, B. Ségard, and P. Glorieux, "Polarisation dynamics of monomode Nd^{3+}:YAG lasers with Cr^{4+} saturable absorber: influence of the pump polarisation," Opt. Commun. **196**, 257–268 (2001).
15. G. Verschaffelt, G. Van der Sande, J. Danckaert, B. Ségard, P. Glorieux, and T. Erneux, "Delayed polarization dynamics in Nd^{3+}-doped yttrium-aluminum-garnet lasers," Phys. Rev. A **77**, 063801 (2008).
16. K. Otsuka and T. Ohtomo, "Polarization properties of laser-diode-pumped micro-grained Nd:YAG ceramic lasers," Laser Phys. Lett. **5**, 659–663 (2008).
17. K. Otsuka, "Polarization-dependent intensity noise in a microchip solid-state laser with spatially coherent polarization vector fields," Opt. Lett. **37**, 4287–4289 (2012).
18. K. Otsuka and S.-C. Chu, "Microchip solid-state cylindrical vector lasers with orthogonally polarized dual laser-diode end pumping," Opt. Lett. **38**, 1434–1436 (2013).
19. S. Zhang, Y. Tan, and S. Zhang, "Effect of gain and loss anisotropy on polarization dynamics in Nd:YAG microchip lasers," J. Opt. **17**, 045703 (2015).
20. H. Chen, S. Zhang, and Y. Tan, "Effect of pump polarization direction on power characteristics in monolithic microchip Nd:YAG dual-frequency laser," Appl. Opt. **55**, 2858–2862 (2016).
21. J. T. Lin and W. A. Gambling, "Polarisation effects in fibre lasers: phenomena, theory and applications," Proc. SPIE **1373**, 42–53 (1990).
22. S. Bielawski, D. Derozier, and P. Glorieux, "Antiphase dynamics and polarization effects in the Nd-doped fiber laser," Phys. Rev. A **46**, 2811 (1992).
23. R. Leners, P. Françcois, and G. Stephan, "Simultaneous effects of gain and loss anisotropies on the thresholds of a bipolarization fiber laser," Opt. Lett. **19**, 275–277 (1994).
24. P. A. Khandokhin, Y. I. Khanin, Y. A. Mamaev, N. D. Milovskii, E. Y. Shirokov, S. Bielawski, D. Derozier, and P. Glorieux, "Low-frequency dynamics of a class B laser with two elliptically polarised modes," Quantum Electron. **28**, 502 (1998).
25. J. Ma and J. Dong, in *Advances in Optical Materials,* (Optica Publishing Group, 2011), p. ATuB27.
26. E. Lacot, F. Stoeckel, and M. Chenevier, "Dynamics of an erbium-doped fiber laser," Phys. Rev. A **49**, 3997 (1994).
27. M. Brunel, O. Emile, M. Alouini, A. Le Floch, and F. Bretenaker, "Experimental and theoretical study of longitudinally monomode vectorial solid-state lasers," Phys. Rev. A **59**, 831 (1999).
28. T. Chartier, F. Sanchez, and G. Stéphan, "General model for a multimode Nd-doped fiber laser. I: Construction of the model," Appl. Phys. B **70**, 23–31 (2000).
29. S. De, A. El Amili, M. Alouini, and F. Bretenaker, "Theoretical and experimental analysis of intensity noise correlations in an optically pumped, dual-frequency Nd:YAG laser," J. Opt. Soc. Am. B **30**, 2830–2839 (2013).
30. M. Brunel, A. Amon, and M. Vallet, "Dual-polarization microchip laser at 1.53 μm," Opt. Lett. **30**, 2418–2420 (2005).